Development 138, 2457-2465 (2011) doi:10.1242/dev.060335

Topoisomerase IIβ is required for lamina-specific targeting of retinal ganglion cell axons and dendrites

Linda M. Nevin, Tong Xiao, Wendy Staub and Herwig Baier*

SUMMARY

The specific partnering of synaptically connected neurons is central to nervous system function. Proper wiring requires the interchange of signals between a postmitotic neuron and its environment, a distinct pattern of transcription in the nucleus, and deployment of guidance and adhesion cues to the cell surface. To identify genes involved in neurite targeting by retinal ganglion cells (GCs), their presynaptic partners in the retina, and their postsynaptic targets in the optic tectum, we undertook a forward genetic screen for mutations disrupting visual responses in zebrafish. This rapid primary screen was subsequently refined by immunohistochemical labeling of retinal and tectal neurites to detect patterning errors. From this unbiased screen, the *notorious* (*noto*) mutant exhibited the most specific phenotypes: intact retinal and tectal differentiation but multiple neurite targeting defects in the retinal inner plexiform layer (IPL) and tectal neuropil. Positional cloning and morpholino phenocopy revealed that the mutation disrupts Topoisomerase IIβ (Top2b), a broadly distributed nuclear protein involved in chromatin modifications during postmitotic differentiation. Top2b-DNA interactions are known to regulate transcription of developmentally important genes, including axon guidance factors and cell adhesion molecules, but a specific role in local synaptic targeting has not been previously described. The neurite targeting defects among GC axons are largely restricted to crossovers between sublaminae of a specific layer, SFGS, and were shown by mosaic analysis to be autonomous to the GC axons. The *noto* mutant provides the first example of the importance of an epigenetic regulator, Top2b, in the intricate series of events that lead to a properly wired visual system.

KEY WORDS: Neurite targeting, Topoisomerase, Retina, Tectum, Zebrafish

INTRODUCTION

Throughout the visual system, axons and dendrites form layered arrays of connections (Huberman et al., 2010). Each layer (or lamina) is composed of synapses with similar functional specializations. In the retina, information extracted from the visual scene is transmitted via morphologically discrete layers of synapses, which correspond to parallel processing streams (Roska and Werblin, 2001). In zebrafish larvae, retinal bipolar cells (BCs), amacrine cells (ACs) and ganglion cells (GCs) form synapses across at least nine sublaminae of the inner plexiform layer (IPL) (Nevin et al., 2008). The majority of GCs project their axons to the optic tectum, another laminated structure. Each GC axon innervates one of six 'retinorecipient' layers in the tectal neuropil, where it forms a planar arbor (Xiao et al., 2005; Nevin et al., 2010). The postsynaptic tectal neuron dendrites also show diverse laminar selectivity, suggesting that GC axons in different laminae have molecularly and functionally distinct postsynaptic partners (Meek and Schellart, 1978; Nevin et al., 2008; Scott and Baier, 2009; Robles et al., 2011).

Although the number of cell-surface proteins implicated in laminar targeting is growing, upstream players regulating transcription of these genes have not been identified. Studies of neural differentiation and activity-dependent synaptic plasticity have begun to paint a complex picture of transcriptional regulation (Polleux et al., 2007; Flavell and Greenberg, 2008; Alberini, 2009). Transcription factors collaborate with epigenetic regulators that modify the structure and accessibility of regions of DNA to the transcriptional machinery. The accessibility of a DNA template to transcription can change following modification of a number of topological parameters: location within the nucleus (Martins and Krawetz, 2007), the types of histones present (Ju et al., 2006), acetylation of local histones (Weaver et al., 2004), methylation of cytosines in the template (Levenson et al., 2006) and local looping of the DNA strand (Sano et al., 2008).

Topoisomerase IIβ (Top2b) has recently emerged as an epigenetic regulator of transcription in later stage neural development (Tsutsui et al., 2001; Lyu et al., 2006). Like all topoisomerases, Top2b uses a strand-passing mechanism to resolve topological problems in DNA; this role in chromatin organization might influence rates of transcription at target sites. Using a forward genetic approach, we have discovered that the zebrafish *top2b* gene has an important role in the fine targeting of visual system neurites to their synaptic laminae. A splice-site mutation in this gene causes GC dendrites within the IPL and GC axons within the tectal neuropil to trespass between laminae, while sparing other features of cellular architecture and axon pathfinding. We demonstrate that Top2b acts within retinal clones to target GC axons to sublaminae within a single tectal lamina, stratum fibrosum et griseum superficiale (SFGS), suggesting that *top2b* has a GC-autonomous function in regulating the expression of target recognition molecules.

MATERIALS AND METHODS

Wild-type strains and transgenic lines

Adult zebrafish from the TL and WIK strains were maintained in our fish facility at the University of California, San Francisco (UCSF). All procedures adhered to the rules of animal use set by the National Institutes of Health and UCSF. Transgenic lines, generated and maintained in TL, were *Pou4f3:mGFP* [*Tg*(*Pou4f3:gap43-GFP*)*s*273*t*] (Xiao et al., 2005), *Pax6:mGFP* [*Tg*(*Pax6-DF4:gap43-GFP*)*s*220*t*] (Kay et al., 2001) and

Department of Physiology, University of California, San Francisco, 1550 4th Street, San Francisco, CA 94158-2722, USA.

*Author for correspondence (herwig.baier@ucsf.edu)

Accepted 6 April 2011

BGUG [*Tg*(*Pou4f3:Gal4,UAS:mGFP*)*s318t]* (Xiao and Baier, 2007). Larvae used live for confocal imaging were raised in phenylthiourea (0.2 mM, Sigma-Aldrich) to block pigmentation.

Forward genetic screen

Detailed procedures of our N-ethyl-N-nitrosourea (ENU) mutagenesis screen have been previously described (Muto et al., 2005). Forty visually impaired mutants from this screen were investigated histologically for neurite targeting defects in the retina and tectum at 5 days postfertilization (dpf), as previously described (Nevin et al., 2008). Primary antibodies used for screening were: mouse anti-Parvalbumin (1:1200, Chemicon); rabbit anti-PKC β1 (1:800, Santa Cruz Biotechnology); and mouse Zrf3 (1:250, Oregon Monoclonal Bank). Antibodies used in follow-up studies were: goat anti-ChAT (1:50, Chemicon) rabbit anti-GFP antibody (1:4000, Molecular Probes); and mouse anti-HuC/D (1:400, Molecular Probes). TUNEL reagent (Roche) was used according to the manufacturer's protocol, with amplification of signal by secondary labeling with Alexa Fluor 488 anti-fluorescein antibody (Molecular Probes).

Identification of the *noto* mutation

Established linkage mapping methods were used to locate the *noto*^{s380} mutation in the genome (Muto et al., 2005). *noto* heterozygotes (in the TL strain) were crossed with fish from the highly polymorphic WIK strain, and adult TL/WIK *noto* heterozygotes were bred repeatedly to generate TL/WIK recombinant wild-type and mutant larvae. Recombination events at microsatellites and other sequence polymorphisms from established panels (Kwok et al., 1998; Shimoda et al., 1999; Woods et al., 2000) and additional markers of our design including marker 12 (from GenBank clone BX927411; forward primer: TGTGCATGTAACATTGACTGTAGACT; reverse primer: AGTCACACCTGCTACACTAGTTATTC), were scored in the WIK/TL recombinant mutant larvae. For candidate gene sequencing, RNA samples from wild-type and mutant larvae were isolated using TRIzol reagent (Invitrogen)/chloroform-based extraction. cDNAs from each RNA sample were reverse transcribed using the 3′ RACE cDNA Synthesis Kit (Clontech). Wild-type and mutant coding sequences of candidate genes were compared using Sequencher software (Gene Codes Corporation).

Morpholino phenocopy of the *noto* mutation

An antisense morpholino (TTTATCTGCTATAAGCTCACCTGCA) targeting the *top2b* exon 11 donor splice site, and a control morpholino with a 5-base sequence mismatch (TTaATgTGCTATAAcCTCAgCTcCA, lower case indicates mismatched bases) were designed and manufactured by GeneTools. These were dissolved at a concentration of 1 mM in water with Phenol Red dye (Sigma-Aldrich). Morpholino solutions were injected with a picospritzer into the yolks of wild-type *BGUG* embryos at the 1- to 4-cell stage. A dose of 1 pmole/embryo was identified as half-lethal (~50% survival); 0.5 pmole, 1 pmole or 1.5 pmole were used in subsequent experiments. For imaging, injected embryos were raised to 5 dpf, sorted for GFP expression, mounted in agarose and imaged. RT-PCR (described above) with 2 and 5 dpf control and morphant fish was used to confirm the morpholino targeting.

RNA in situ hybridization

A 1.3 kb fragment (forward primer: TTGCAGCCTGGAACAAAGCTC-AAG; reverse primer: AGCAAGAAGCGAAAGCAGTCAAGC) of *top2b* was cloned into the pCRII-TOPO vector (Invitrogen). Sense and antisense digoxigenin-labeled RNA probes were made by in vitro transcription using an RNA labeling kit (Roche). Hybridization and staining were performed on 1-6 dpf larvae, according to methods previously described (Smear et al., 2007).

Image collection and analyses

Fluorescence images were collected using a Zeiss LSM 5 Pascal confocal microscope, with a 40× oil objective for slides and a 40× water immersion objective for live fish. Processing and quantification of images of retina and tectum sections have been described (Nevin et al., 2008). Live fish were mounted in agarose according to a standard protocol (Smear et al., 2007). Confocal stacks were processed to projected 3D images using ImageJ software. Several images with more than one GC axon were painted to generate one stack for each axon; individual axons were then assigned one channel in an RGB scheme to generate multicolor projected images. For the GC axon morphometry study, stacks were imported into NeuronStudio (Wearne et al., 2005) for three-dimensional tracing and length/branching quantifications.

Blastula stage transplantations

Chimeric larvae were generated using standard methods (Gosse et al., 2008). *Pou4f3:mGFP*+, *noto* heterozygous adults were incrossed to generate donors, and non-transgenic *noto* heterozygotes were incrossed to generate hosts. Donor embryos were labeled by injection at the 1- to 4-cell stage with Alexa 555-dextran (MW 10,000, 1% w/v each, Molecular Probes Invitrogen). At the blastula stage, small numbers (5-15) of cells were transplanted from donor to host animal pole. At 24 hpf, transplanted hosts were sorted for red fluorescent clones in the eye. Chimeras with retinal clones, and their corresponding donors, were raised to 5 dpf and scored as either wild type or mutant; hosts with donor-derived GC axons in a donor clone-free tectum were imaged.

RESULTS

The *noto* mutation impairs neurite targeting in the IPL

A primary mutagenesis screen of ~2000 genomes (Muto et al., 2005) yielded a collection of visually impaired mutants, which subsequently were sectioned and stained by immunohistochemistry with retinal and tectal cell-type markers. We became particularly interested in the blind *notorious* (*noto*) mutant owing to its specific neurite targeting defects. *noto* mutants had normal morphology and cytoarchitecture; DAPI staining of the retina and tectum showed the wild-type organization of cells (Fig. 1A,G, Fig. 2A,D). In addition, staining with cell type-specific markers indicated that neuron types differentiate appropriately (Fig. 1 and see Figs S1, S2 in the supplementary material) and TUNEL staining showed no striking change in cell death in the retina at 5 dpf (wild type: n=7, mean 0.9 TUNEL+ cells/central section, s.e.m. 0.6; *noto*: n=5, mean 0.6 TUNEL+ cells/central section, s.e.m. 0.4).

Although cell types were properly generated and localized, the local targeting of retinal neurites was perturbed (Fig. 1 and see Fig. S1 in the supplementary material). For example, Parvalbumin (Parv)+ AC neurites in the wild-type 5 dpf retina target IPL sublaminae s25, s45 and s85; these sublaminae are located at 25%, 45%, 85% of the distance from inner to outer edge of the IPL, respectively (Nevin et al., 2008). In the mutant, Parv+ AC neurites appropriately targeted strata in the two halves of the IPL, but the bands of immunoreactivity were coarse and the s25 and s45 bands were merged. Analogous errors were made by other IPL neurites, including Protein kinase C (PKC)+ bipolar cell axons, *Pou4f3:mGFP*+ GC dendrites, and *Pax6:mGFP*+ and choline acetyltransferase (ChAT)+ AC neurites. Notably, the targeting of *Pax6:mGFP*+ and ChAT+ AC neurites was nearly normal, but the fine sublamination of these neurites into doublet bands (e.g. s40/s45 for *Pax6:mGFP*) was lost.

The IPL sublamination errors in the mutant were quantified by scoring the number of distinct PKC+, *Pou4f3;mGFP*+ and Parv+ bands in the IPL of multiple retinas (Nevin et al., 2008). As shown in Fig. 1M, wild type and mutant each had a reproducible number of IPL sublaminae, and the observed differences were statistically significant (for all three comparisons: n=10 wild-type and 10 mutant retinas, P<0.01). These sublamination errors were more pronounced, and the IPL more disorganized, in older (7 dpf) mutants (see Fig. S2 in the supplementary material). We conclude that mutant neurites fail to target their correct sublaminae and that

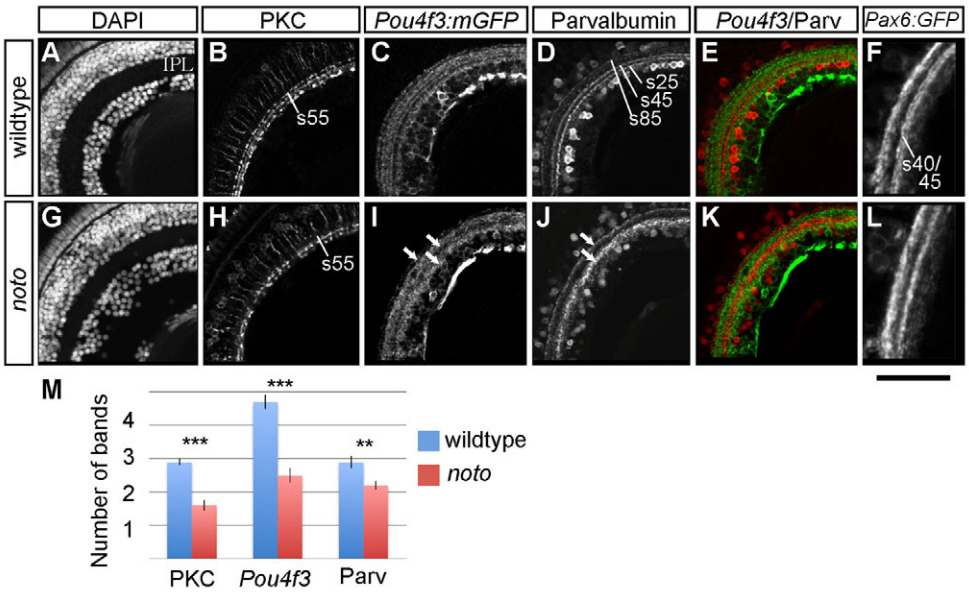

Fig. 1. Fine neurite targeting is disrupted in the 5 dpf *noto* mutant inner plexiform layer (IPL). (**A-L**) Representative sections of wild-type (A-F) and mutant (G-L) zebrafish retina. DAPI nuclear stain shows the cellular organization of the retina, including location and width of the IPL (A,G). Protein kinase C (PKC)+ bipolar cells (BCs) project terminals to three IPL sublaminae in wild type (B); in the mutant, outermost sublamina *s55* is sparsely innervated (H). *Pou4f3:mGFP*+ ganglion cell (GC) dendrites innervate five sublaminae in wild type (C); arrows in I show three coarse sublaminae in the mutant IPL (I). Parvalbumin (Parv)+ amacrine cells of the inner nuclear layer (INL) and ganglion cell layer (GCL) project neurites to three sublaminae (*s25*, *s45* and *s85*) in wild type (D); arrows in J show two broad sublaminae in the mutant (J). Merged images show the relative positions of *Pou4f3:mGFP*+ and Parv+ IPL sublaminae (E,K). *Pax6:mGFP*+ amacrine cells project neurites to two IPL bands; the inner band is actually the two fine sublaminae *s40* and *s45* (F,L). The *s40/s45* division is lost in the mutant. Scale bar: 50 μm for A-E,G-K; 30 μm for F,L. (**M**) Mean number of distinct bands of PKC, *Pou4f3:mGFP* and Parv immunoreactivity from ten wild-type (blue) and ten mutant (red) retinas. Error bars represent s.e.m. $**P<0.01$; $***P<0.00001$.

the mutated gene is important for sublaminar positioning of most, perhaps all, inner nuclear layer (INL) and GC layer (GCL) retinal neurons.

GC axon and tectal neurite targeting are aberrant in the *noto* mutant tectum

The *noto* mutant also has neurite organization defects in the tectal neuropil. In wild type, *Pou4f3:mGFP*+ GC axons innervate three layers, with each axon among this population arborizing in just one of these layers, either the stratum opticum (SO) or one of two sublaminae of the SFGS (Xiao and Baier, 2007). Cryostat sections of the *Pou4f3:mGFP*+ labeled projection in the mutant tectum revealed that the two labeled *GFP*+ sublaminae of SFGS are expanded and that bridges develop between them. The fine targeting of axons to the SO appeared normal in sections of the mutant tectum (Fig. 2A,D, n=10 wild-type siblings, n=15 mutants).

The postsynaptic partners of GC axons are the dendrites of tectal neurons, most of which extend from the cell bodies in the periventricular region of the tectum into strata of the neuropil. Several types of periventricular neurons extend dendrites in a lamina-specific pattern (Meek and Schellart, 1978; Scott and Baier, 2009; Robles et al., 2011). PKC and Parv antisera label two such populations (Nevin et al., 2008). Antibody staining of sections revealed that laminar targeting by these tectal dendrites is severely compromised in *noto* mutants (Fig. 3, n=10 wild-type and mutant larvae each). In contrast to the mutant IPL, in which the wild-type pattern was replaced with a distinct alternate pattern, mutant tectal neurites appeared to have very little or no organization; instead, the neuropil was broadly immunolabeled, suggesting a lack of neurite refinement.

Individual *noto* mutant GC axons show severely impaired laminar targeting

GC axon targeting can be assessed by live confocal imaging of larvae expressing the paired transgenes *Pou4f3:Gal4,UAS:mGFP* (*BGUG*), where the *UAS:mGFP* expression is variegated (Xiao and Baier, 2007), thus labeling a small number of axons. Examination of *BGUG* larval tecta, such as those shown in Fig. S3 in the supplementary material, revealed a highly disorganized SFGS in mutants, suggesting multiple targeting errors, and in just one case, a crossover between SO and SFGS.

We hypothesized that individual mutant GC axons often trespass between the finer layers of SFGS, but very rarely between SO and SFGS. To test this hypothesis and learn more about the morphology of mutant GC axons, we selected larvae with *BGUG* expression in individually distinguishable axons. Wild-type axons in both SO and SFGS projected arbors to narrow bands within the tectum, with cross-sectional widths not exceeding 8 μm (SO: mean 4.5 μm, s.e.m. 1.3, n=4 axons from three fish; SFGS: mean 4.4 μm, s.e.m. 0.3, n=24 axons from 11 fish). Measurements from confocal images of *Pou4f3c:mGFP*+ wild-type larvae enabled us to estimate the width of SO (5 μm) and each sublamina of SFGS (10 μm); individual wild-type axons are therefore confined to strata as thin as, or thinner than, these identified layers. The mutant SO axons imaged were also finely targeted (mean width 3.9 μm, s.e.m. 0.7, n=6 axons from six fish); however, the population of SFGS axons was clearly distinct from wild type. First, we observed a population of GCs in which the unbranched axon extended into one lamina, then crossed into another, usually turning 180 degrees, to elaborate a branched arbor in an antiparallel conformation (see Fig. S4 in the supplementary material); these instances were scored as entry

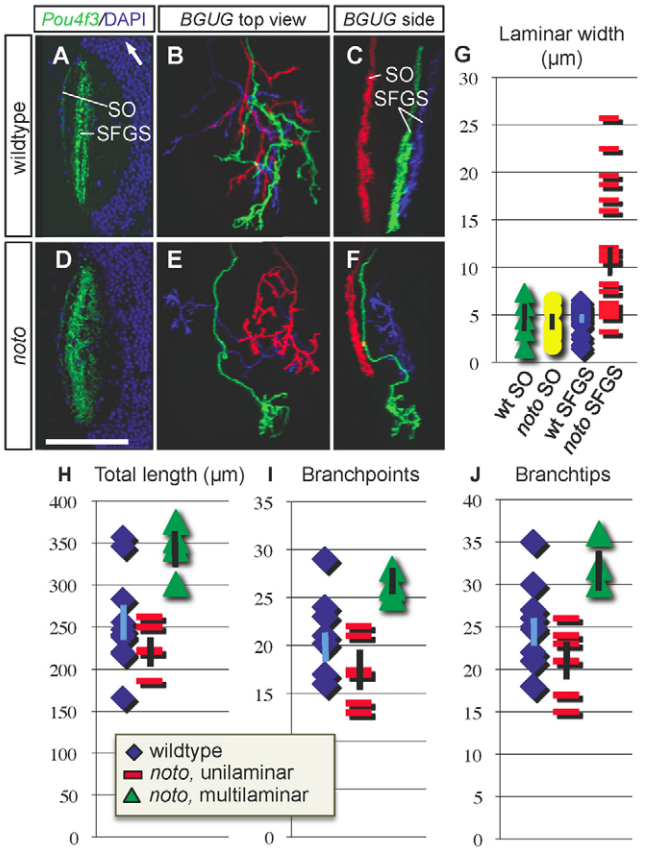

Fig. 2. *noto* mutant ganglion cell (GC) axons project aberrantly between SFGS tectal sublaminae. (**A**,**D**) Representative horizontal sections of wild-type (A) and mutant (D) tectum in *Pou4f3:mGFP*+ 5 dpf zebrafish larvae. GFP is in green, DAPI nuclear stain is in blue. White arrow in A points rostrally. (**B**,**C**,**E**,**F**) Small numbers of GC axons labeled in *BGUG*+ transgenic wild-type (B,C) and mutant (E,F) larvae. Images are projections of confocal stacks in top (B,E) and side (C,F) views. Each red axon lies in SO; blue and green axons innervate SFGS. Both green and blue axons in panel F are wider than 10 μm in side view and scored as multilaminar. Scale bar: 70 μm for A,D; 50 μm for B,C,E,F. (**G**) Scatter graph of side-view widths of wild-type SO (*n*=4), mutant SO (*n*=6), wild-type SFGS (*n*=24) and mutant SFGS (*n*=24) axons in wild type and mutant. (**H-J**) Morphometric analysis of wild-type and mutant *BGUG*+ GC axons. Scatter plots showing total arbor length (H), number of branchpoints (I) and number of branchtips (J) in wild-type (*n*=10), mutant unilaminar (*n*=5) and mutant multilaminar (*n*=3) SFGS axons. Population means are plotted as points, error bars represent s.e.m.

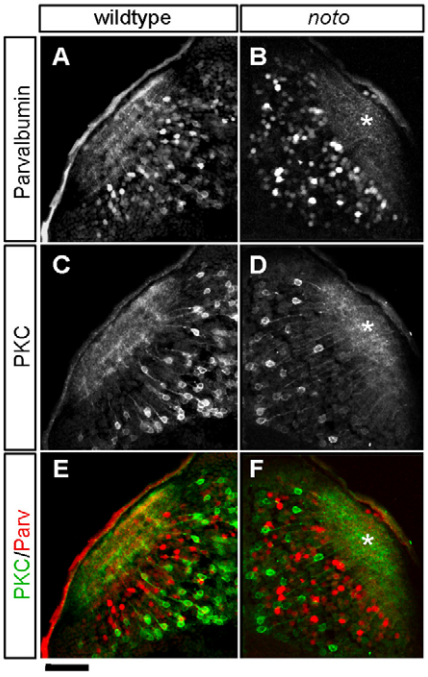

Fig. 3. *noto* mutant tectal neurons have unrefined neuropil projections at 5 dpf. Sections of wild-type (A,C,E) and mutant (B,D,F) zebrafish tectum showing tectal cell populations and their neuropil neurites. Disorganized neuropil in the mutant is marked with asterisks. (**A**,**B**) Wild-type Parvalbumin (Parv)+ tectal neurons project neurites to four laminae in the neuropil; this laminar organization is incomplete in the mutant. (**C**,**D**) Wild-type Protein kinase C (PKC)+ tectal neurons project neurites to three laminae in the neuropil; this laminar organization is lost in the mutant. (**E**,**F**) Merged images showing relative location of laminae. Scale bar: 50 μm.

defects (6 of 24 axons; Fig. 2G). By contrast, wild-type axons always entered and elaborated arbors in the same stratum, as previously reported (Xiao and Baier, 2007).

Although entry defects contribute to the laminar disorganization seen at the population level, most of it probably results from the increased arbor width of the mutant axons. The mean SFGS axon width in the mutants was greater than in wild type (10.8 μm, s.e.m. 1.4, *n*=24 axons from 14 fish; *t*-test with unequal variance, $P<0.0003$); many mutant SFGS axons extended arbors wider than 10 μm and were scored as 'multilaminar' (10 of 24 axons; Fig. 2). Multilaminar axons were clearly different from their wild-type counterparts when viewed from the side; many branches trespassed out of the initially targeted lamina, and sometimes a secondary planar arbor formed. Morphometric analyses (Fig. 2I-K) demonstrated that these multilaminar arbors are of greater length and branch complexity than unilaminar mutant SFGS axons (including those with entry defects). Mean total arbor length, number of branchpoints and number of branchtips were increased in multilaminar axons ~50% above the mean measurement for mutant unilaminar axons (*t*-test, $P=0.004$, 0.005, 0.01, respectively; *n*=5 unilaminar axons and 3 multilaminar axons). However, all mutant SFGS axons measured fell within the wild-type range for these metrics. The modest decrease in size and complexity of unilaminar axons in the mutants might be the result of lamina-specific competition for limiting postsynaptic partners, as the unilaminar axons might face increased competition from multilaminar neighbors in the mutant. Alternatively, *top2b* might be regulating arbor complexity in a GC type-specific manner, limiting branching and extension in some and promoting these processes in others.

The *noto* genetic lesion is a splice-site mutation in topoisomerase-2β

Genetic linkage mapping and positional cloning methods were used with a pool of ~5000 mutant larvae to localize the *noto* mutation to chromosome 19, between T51 marker *fj94f01* to the North and our own marker 12 to the South (see Materials and methods). These and flanking markers from our study are not arranged in contiguous order in the ensEMBL zebrafish genome assemblies Zv7 or Zv8; however, we used the ensEMBL

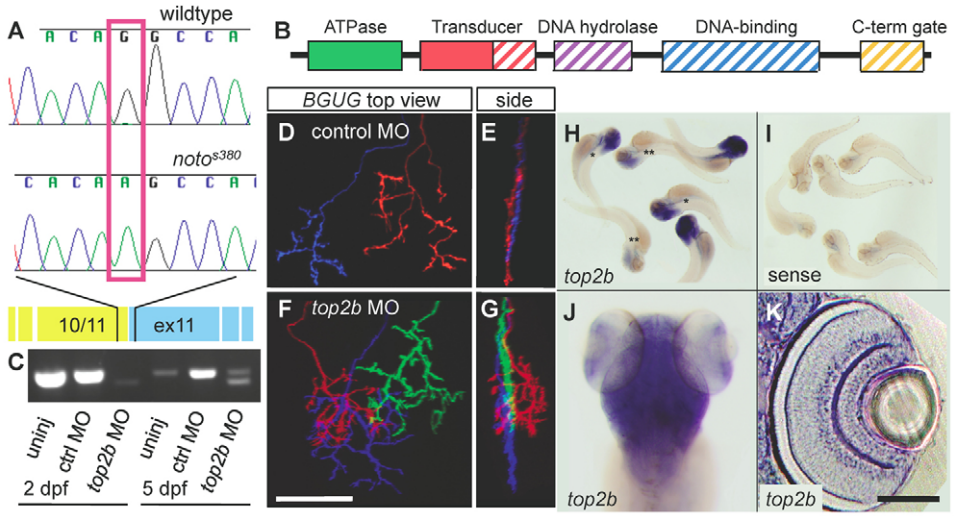

Fig. 4. The *noto* genetic lesion is a nonsense splice site mutation in *top2b*. (**A**) Sequence chromatograms showing the *top2b* exon 11 splice acceptor site in wild-type and mutant zebrafish. The sequence shown is at the intron-exon border shown in yellow and blue, respectively. (**B**) Schematic of the functional domains of Top2b protein. Solid colored regions are preserved in the predicted mutant protein; diagonal lines indicate the truncated portion. (**C**) RT-PCR-amplified *top2b* fragments from uninjected, control morphant and *top2b* morphant fish at 2 and 5 dpf. Morpholino oligonucleotide (MO) knockdown results in a truncated cDNA; both the full-length and truncated products can be detected by 5 dpf. (**D-G**) Ganglion cell (GC) axons from *BGUG*+ larvae in morpholino phenocopy experiment. (D,E) Top (D) and side (E) views of two SFGS axons from a control morphant. (F,G) Top (F) and side (G) views of three SFGS axons from an antisense *top2b* morphant; red axon is multilaminar. Scale bar: 50 μm. (**H-K**) In situ hybridization showing expression of *top2b* in 4 dpf larvae. (H) Antisense probe labels brain and eye. Unlabeled larvae are homozygous wild type (+/+), single asterisk indicates $noto^{+/-}$, double asterisk indicates $noto^{-/-}$. (I) Sense probe labeling is minimal. (J) Magnified dorsal view of antisense labeling. (K) Higher magnification view of sectioned retina, showing strong expression in amacrine cells (ACs) and GCs. Scale bar: 250 μm for H,I; 150 μm for J; 50 μm for K.

physical map in combination with our results to generate a ~2 Mb region of candidate genes. This region included the full coding sequence of *top2b*. Wild-type and mutant *top2b* were cloned in fragments; one fragment, spanning exons 9 to 20, was ~140 bp smaller in mutant cDNA. Sequencing revealed that the mutant fragment lacked exon 11. Genomic regions flanking each end of the exon were amplified and sequenced, confirming the presence of a G-to-A transition in the splice acceptor sequence of exon 11 (Fig. 4A). The alternatively spliced product is frame-shifted relative to wild type, and leads to an early stop codon in exon 12 (position 1853) of the 35-exon (4857 bp) cDNA. Top2b is a DNA-modifying enzyme that binds two double helices, cleaves one (the g-strand, for 'gate') and passes the other (the t-strand, for 'transfer') through the break, and then re-anneals the cleaved strand. Although the mutant *top2b* gene product retained the N-terminal ATPase region, which initially binds the t-strand, and part of the adjacent domain that transduces the power of ATP hydrolysis into a conformational change, it is predicted to lack the domains necessary to bind and cleave the g-strand, as well as the exit gate for the t-strand (Fig. 4B). Although this truncated protein is unlikely to retain topoisomerase activity, it is unclear whether the mutation results in a complete loss of function, as some wild-type splice variants might still be produced.

To confirm that the *noto* locus encodes the *top2b* gene, we phenocopied the mutant by antisense morpholino oligonucleotide (MO) gene knockdown in *BGUG*-transgenic fish. The *top2b* MO was targeted to the exon 11 splice donor site, closely simulating the $top2b^{s380}$ mutation; a 5 bp mismatched MO was used as a control. Injected embryos were raised to 5 dpf and imaged to detect possible aberrations in axon targeting. We found that injected embryos were extremely sensitive to the *top2b* MO (but not to the control MO); a concentration of 1 pmole/embryo was lethal to ~50% of the fish. To verify targeting and to monitor degradation of the MO in the embryos injected with this dose, *top2b* cDNAs were cloned and sequenced from 2 and 5 dpf control morphant and *top2b* morphant fish. As expected, controls had the wild-type product, whereas *top2b* morphant cDNAs had the aberrantly spliced product at 2 dpf (Fig. 4C). At 5 dpf, however, *top2b* morphant cDNA contained a small amount of wild-type *top2b* in addition to the truncated form. We conclude that degradation of the MO allows recovery of *top2b* splicing by 5 dpf. The transient nature of the knockdown might therefore confound our ability to phenocopy the neurite targeting defects seen in mutants at 5 dpf.

Nevertheless, the multilaminar arbor phenotype seen in mutants was recapitulated in a subset of the morphant SFGS axons (2 of 17 axons, from six MO-injected fish, mean width 9.5 μm, s.e.m. 0.8 μm). Although the percentage of defective *tob2b* morphant axons was small, the defects were pronounced; the two aberrant arbors we observed had cross-sectional widths of 25 and 38 μm, falling 20 and 33 standard deviations, respectively, outside the control mean. Injections with the control MO into *BGUG*+ fish did not cause any targeting defects in 23 SFGS axons imaged from eight larvae (Fig. 4D-G; mean arbor width 4.9 μm, s.e.m. 0.2 μm). Notably, the IPL sublamination defects observed in mutants were not seen in the morphants. If a small number of IPL neurites (equivalent to the fraction of multilaminar GC axons in morphants) were aberrantly targeted, their defects might be masked by the rest of the population. Moreover, *BGUG*+ GC dendrites have variable, dynamically changing morphologies (Mumm et al., 2006); IPL sublamination errors, if any, of individual GCs can therefore not be scored, a limitation that applies to both mutants and morphants.

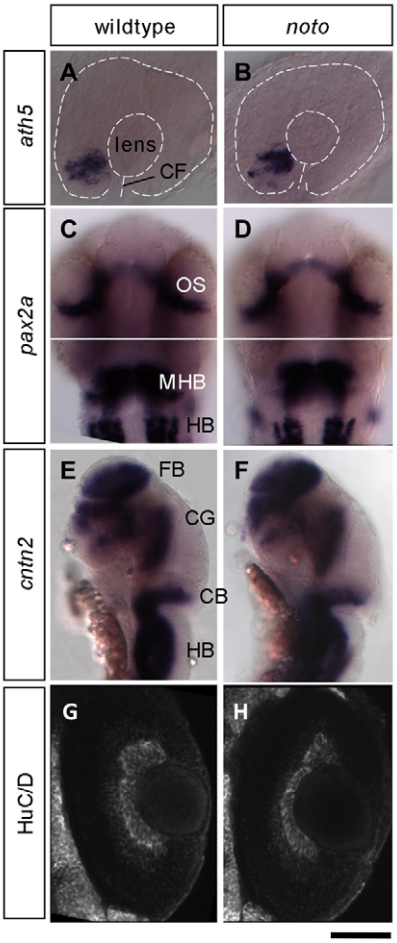

Fig. 5. Expression patterns of early brain and eye development are preserved in *noto* mutants. (**A**,**B**) In situ hybridization with *ath5* antisense probe at 28 hpf shows normal progression of neurogenesis in the wild-type and mutant zebrafish retina. Border of eye, lens and position of the choroid fissure (CF) are indicated by dashed lines. (**C**,**D**) *pax2a* expression at 28 hpf shows grossly normal development of the optic stalk (OS), midbrain-hindbrain boundary (MHB) and neurons of the hindbrain (HB) in both wild type and mutant. (**E**,**F**) *cntn2* expression at 36 hpf shows grossly normal development of the forebrain (FB), several cranial ganglia (CG), the cerebellum (CB) and hindbrain (HB) in both wild type and mutant. (**G**,**H**) Confocal images of whole-mount HuC/D antibody-stained 48 hpf embryos. A similar population of HuC/D labeled ganglion cells (GCs) has developed in wild type (G) and mutant (H). Scale bar: 40 μm for A,B; 100 μm for C-F; 30 μm for G,H.

top2b mRNA is broadly expressed at early stages and becomes restricted to the CNS later

To find clues for the role of *top2b* in larval zebrafish development, we used RNA in situ hybridization to track expression of *top2b* during development. At 1 dpf, *top2b* was expressed broadly throughout the embryo (see Fig. S5A,D in the supplementary material). Thereafter, from 2 to 6 dpf (the last time point tested), expression was restricted to the head region, and was ubiquitous in the brain (Fig. 4H-K and see Fig. S5 in the supplementary material). By 4 dpf, the gene was expressed in the retina, but appeared to be absent from the photoreceptors, weak in the outer two-thirds of the INL and strong in the innermost INL and in the GCL. This pattern indicates strongest expression in ACs and GCs. Staining was performed on progeny from incrossed *noto* heterozygotes; at each stage, ~25% of the stained embryos or larvae were weakly labeled. Figure 4H shows a representative collection of stained 4 dpf larvae; after imaging, the individual fish shown were genotyped for the *noto* mutation. As shown, the darkest staining accurately predicted a homozygous wild-type genotype, heterozygotes were stained at an intermediate level and mutants had dim staining. The reduction of *top2b* in *noto* mutants and heterozygotes indicates nonsense-mediated decay of the mutant RNA.

Top2b does not affect early stages of neural patterning and differentiation

To explore the role of *top2b* in nervous system patterning, we assessed the expression of a set of early domain markers at 28-48 hours postfertilization (hpf, Fig. 5) (Warren et al., 1999; Kay et al., 2001; Thisse et al., 2001). Expression of *ath5* (*atoh7*), encoding a basic helix-loop-helix transcription factor required for generating GCs, was prominent at 28 hpf in ventronasal retina in both wild type and *noto* mutants. By 48 hpf, the mutant GCL was populated with HuC+ neurons, indicating that GCs differentiate in a normal time course. Early brain development was also grossly preserved. Expression of the homeobox transcription factor *pax2a* in the optic stalk, choroid fissure, midbrain-hindbrain boundary, and a collection of hindbrain neurons was maintained in 28 hpf mutants. At 36 hpf, expression of the surface immunoglobulin *cntn2* could be observed in the telencephalon, the trigeminal, facial and acoustic/anterior lateral line ganglia, cerebellum and hindbrain of both wild-type and mutant embryos. This survey of developmental markers indicates that the neurite targeting phenotypes observed in the mutant do not represent a failure to generate basic cell types or brain structures.

Top2b has a specific, retina-autonomous role in GC axon laminar targeting

The expression of *top2b* might be important within the GCs to supply the axon with the correct complement of guidance receptors, or might act within tectal cells to create a proper scaffold. We addressed this question of cell autonomy using chimeric analyses. Blastula stage transplantation of undifferentiated cells from the eye fields of *Pou4f3:mGFP*+ donors into the same region of non-transgenic expressors was used to generate chimeric blastulae, which were raised to 5 dpf. In these larvae, we saw small populations of donor-derived axons arborized in a host tectum (Fig. 6). In chimeras in which wild-type axons innervated a mutant tectum, laminar targeting was free of errors. By contrast, mutant axons innervating the SFGS lamina of wild-type tectum appeared disorganized and trespassed between sublaminae. We quantified our findings in a subset of chimeras with individually distinguishable axons in SFGS; 13 such wild type-derived axons in mutant tecta showed the expected fine targeting, whereas multilaminar arbors were observed in 2 of the 10 distinct mutant-derived axons innervating wild-type tecta (wild type→*noto:* n=13 axons in four fish, mean arbor width 4.8 μm, s.e.m. 1.0; *noto*→wild type: n=10 axons in five fish, mean width 7.4 μm, s.e.m. 7.1 μm). These multilaminar arbor widths were 13 and 26 μm, falling 6 and 14 standard deviations from the mean wild-type arbor, respectively. We conclude that the *top2b* genotype of the transplanted retinal clone, rather than of the host tectum, determines the lamination phenotype of the GC axon.

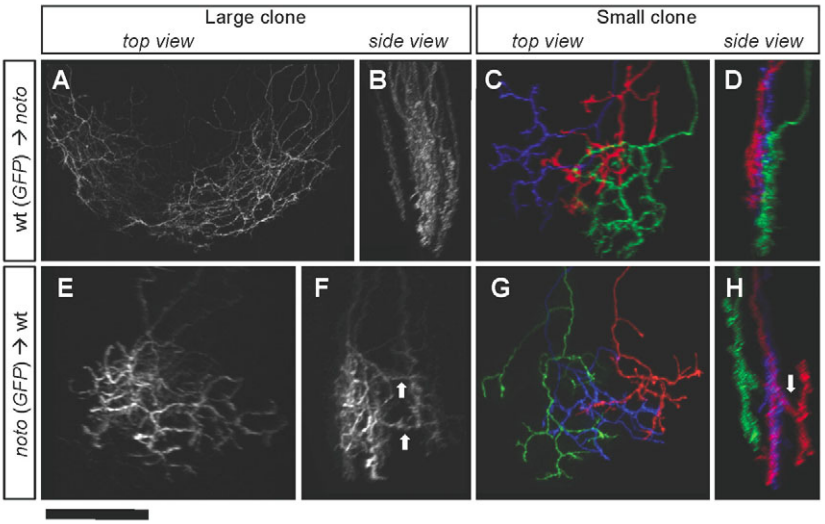

Fig. 6. *noto* mutant ganglion cell (GC) sublamination defects are retina-autonomous. (**A-D**) GC axons derived from wild-type zebrafish donors, innervating mutant tecta. (A,B) Top and side views of a large cluster of axons, including one SO and many SFGS axons, showing orderly sublamination. (C,D) Top and side views of individual GC axons, showing fine sublamination within SFGS. (**E-H**) GC axons derived from mutant donors, innervating wild-type tecta. (E,F) Top and side views of a large cluster of SFGS axons, showing disordered sublamination; arrows show laminar crossovers. (G,H) Top and side views of three SFGS axons. Red axon is multilaminar; arrow shows crossover. Scale bar: 50 μm.

DISCUSSION

Our forward genetic screen successfully uncovered a mutant with pronounced neurite laminar targeting defects despite normal cytoarchitecture, cell differentiation and formation of long-range connections. Marker analysis indicated that a wide range of neural cell types are formed at the right time and place in the retina and tectum. In particular, GC differentiation is initiated on time, as shown by *ath5* expression, and a properly developed GCL, immunostained against HuC, appears by 48 hpf. Despite apparently normal cellular organization, all seven neural populations examined show some aberration in the laminar targeting of neurites in the retina and/or tectum. Defects were observed in the axons of a population of bipolar cells (PKC+), dendrites of three populations of amacrine cells (Parv+, ChAT+ and *Pax6:mGFP*+), and both the dendrites and axons of *Pou4f3:mGFP*+ GCs. Two populations of tectal neurites (Parv+ and PKC+) also lack the normal precision of laminar organization within the neuropil. In every case, neurite pathfinding to the retinal or tectal neuropil is preserved, and the wild-type laminar pattern is usually approximated, but fine targeting is disrupted. As in the mouse *top2b* mutant (Yang et al., 2000; Lyu and Wang, 2003), the earliest steps of development – proliferation and mitotic exit – are preserved in zebrafish *noto* mutants. In the mouse *Top2b* knockout, laminar organization of neuronal cell bodies in the cortex and pathfinding of some motor and sensory axons are also disrupted, suggesting additional defects in neural patterning not seen here in the zebrafish visual system.

Closer examination in the *BGUG*+ line revealed that some mutant GC axons branch exuberantly and trespass SFGS sublaminae. These defects were shown by chimeric analyses to be retina-autonomous, suggesting a role for *top2b* in regulating expression of targeting factors within SFGS-projecting GCs. However, because transplantation generates retinal clones containing all cell types, *top2b* might instead act within other retinal neurons, which in turn might instruct the synaptic choices of neighboring *BGUG*+ GCs. This more circuitous mechanism would probably be independent of synaptic transmission, as various disruptions and blockade of synaptic signaling between retinal neurons do not affect the laminar pattern of SFGS innervation (Nevin et al., 2008). In either case, the axon targeting defects observed are consistent with a lack of repulsion from inappropriate laminae; perhaps these GC axons have lost the ability to detect a repulsive factor. How can a broadly expressed gene like *top2b* contribute to a cell type-specific laminar choice? First, the Top2b protein probably cooperates with many other transcriptional regulators to coordinate transcription; these other factors probably show cell type-specific expression. Second, although *top2b* gene expression is broad, protein activation might not be; Top2b can be phosphorylated by numerous intracellular signals, including Casein kinase II, PKC, Protein kinase A (PKA), Extracellular signal-regulated kinase (ERK) and Mitogen-activated protein kinase (MAPK) (Ju and Rosenfeld, 2006).

Gene expression data suggest that Topoisomerase IIa (Top2a) and Top2b have divergent roles. Both gene products are broadly expressed at 1 dpf; *top2a* RNA is detectable in the head and neural tube (Dovey et al., 2009), whereas *top2b* probe labels the whole embryo. After this time point, *top2a* expression persists in proliferative zones (Dovey et al., 2009), whereas *top2b* becomes restricted to postmitotic neurons. The zebrafish data corroborate observations from mammals; *top2b* has been shown in developing rat cerebellum to be expressed just as *top2a* diminishes, as neurons exit the cell cycle and begin to differentiate morphologically (Tsutsui et al., 2001). The refinement of zebrafish *top2b* to brain and retina by 2 dpf coincides with the onset of local neurite targeting by ACs in the IPL and GCs in the tectal neuropil; a thin IPL plexus is visible beginning at ~42 hpf (Godinho et al., 2005), whereas the first GC axons reach rostral tectum at 48 hpf (Stuermer, 1988; Burrill and Easter, 1995). Combined, these observations suggest that the role of Top2a in neurons is predominantly in proliferation, whereas the function of Top2b continues into neurite targeting phases.

The most parsimonious explanation for the *noto* phenotypes stems from the known molecular function of type II topoisomerases: altering DNA topology via the passage of one double helix through another. Because of the length of chromosomes, and the association of genomic DNA with multiple proteins, local supercoiling cannot be resolved or altered by twisting the full chromosome; topoisomerases make local changes to create desirable topology. Top2a appears to be particularly important for the untangling of chromosomes prior to segregation during mitosis (Dovey et al., 2009), and perhaps has some function in transcription also (Mondal and Parvin, 2001; Mondal et al., 2003). Top2b, by contrast, appears dispensable for proliferation but involved in several facets of transcription. Top2b protein is associated with RNA polymerase

(Wang, 1991), histone deacetylases (Tsai et al., 2000; Johnson et al., 2001) and human chromatin remodeling complex hACF (LeRoy et al., 2000). Possibly, each of these DNA-modifying enzymes might cooperate with topological modifications by Top2b to adjust the availability of target genes for transcription. The sites of action of Top2b are not distributed randomly throughout the genome; mammalian Top2b might preferentially associate with matrix attachment regions (MARs) (Martins and Krawetz, 2007; Sano et al., 2008). Conformational changes at or near MARs might position sections of chromatin in regions with higher or lower transcriptional activity. Alternatively, the double strand breaking activity of Top2b might act as a marker to recruit other transcriptional regulators, as has been shown for the localization of Parp1 to the promoters of several estrogen receptor target genes (Ju et al., 2006). This varied collection of mechanisms suggests that the ability of Top2b to break and passage double stranded DNA is integrated in multiple ways by distinct transcriptional cascades.

The neurite targeting phenotypes of the *noto* mutant support a role for Top2b in the fine coordination of transcription of a small number of targets, as a broad abrogation of transcription would result in more severe developmental defects. Gene expression analyses of rat cerebellar cultures treated with a Top2b inhibitor and of the brains of mouse *Top2b* mutants reveal that a small collection of genes (1-4% in one study) are up- or downregulated by Top2b. The pool of targets is enriched with developmentally important genes, including guidance factors, adhesion molecules and synapse components (Tsutsui et al., 2001; Lyu et al., 2006). The identification of analogous targets in zebrafish is an appealing area for further study. It seems likely that the tuning of expression of a number of these targets cooperatively guides visual system neurites to precise synaptic laminae.

Acknowledgements
Thanks to Joel Bordayo for technical support for the GC axon morphometry study, Jeremy Kay for discussions, and the Baier lab screening team. L.M.N. was the recipient of predoctoral fellowships from NSF and the UCSF NIH Vision training grant. This research was funded by NIH grants EY13855 and EY12406 to H.B. Deposited in PMC for release after 12 months.

Competing interests statement
The authors declare no competing financial interests.

Author contributions
L.M.N. performed research, analyzed data and drafted the manuscript. T.X. and W.S. assisted with research. H.B. designed the study and drafted the manuscript.

Supplementary material
Supplementary material for this article is available at
http://dev.biologists.org/lookup/suppl/doi:10.1242/dev.060335/-/DC1

References
Alberini, C. M. (2009). Transcription factors in long-term memory and synaptic plasticity. *Physiol. Rev.* **89**, 121-145.
Burrill, J. D. and Easter, S. S., Jr (1995). The first retinal axons and their microenvironment in zebrafish: cryptic pioneers and the pretract. *J. Neurosci.* **15**, 2935-2947.
Dovey, M., Patton, E. E., Bowman, T., North, T., Goessling, W., Zhou, Y. and Zon, L. I. (2009). Topoisomerase II alpha is required for embryonic development and liver regeneration in zebrafish. *Mol. Cell. Biol.* **29**, 3746-3753.
Flavell, S. W. and Greenberg, M. E. (2008). Signaling mechanisms linking neuronal activity to gene expression and plasticity of the nervous system. *Annu. Rev. Neurosci.* **31**, 563-590.
Godinho, L., Mumm, J. S., Williams, P. R., Schroeter, E. H., Koerber, A., Park, S. W., Leach, S. D. and Wong, R. O. (2005). Targeting of amacrine cell neurites to appropriate synaptic laminae in the developing zebrafish retina. *Development* **132**, 5069-5079.
Gosse, N. J., Nevin, L. M. and Baier, H. (2008). Retinotopic order in the absence of axon competition. *Nature* **452**, 892-895.
Huberman, A. D., Clandinin, T. R. and Baier, H. (2010). Molecular and cellular mechanisms of lamina-specific axon targeting. *Cold Spring Harb. Perspect. Biol.* **2**, a001743.
Johnson, C. A., Padget, K., Austin, C. A. and Turner, B. M. (2001). Deacetylase activity associates with topoisomerase II and is necessary for etoposide-induced apoptosis. *J. Biol. Chem.* **276**, 4539-4542.
Ju, B. G. and Rosenfeld, M. G. (2006). A breaking strategy for topoisomerase IIbeta/PARP-1-dependent regulated transcription. *Cell Cycle* **5**, 2557-2560.
Ju, B. G., Lunyak, V. V., Perissi, V., Garcia-Bassets, I., Rose, D. W., Glass, C. K. and Rosenfeld, M. G. (2006). A topoisomerase IIbeta-mediated dsDNA break required for regulated transcription. *Science* **312**, 1798-1802.
Kay, J. N., Finger-Baier, K. C., Roeser, T., Staub, W. and Baier, H. (2001). Retinal ganglion cell genesis requires lakritz, a Zebrafish atonal Homolog. *Neuron* **30**, 725-736.
Kwok, C., Korn, R. M., Davis, M. E., Burt, D. W., Critcher, R., McCarthy, L., Paw, B. H., Zon, L. I., Goodfellow, P. N. and Schmitt, K. (1998). Characterization of whole genome radiation hybrid mapping resources for non-mammalian vertebrates. *Nucleic Acids Res.* **26**, 3562-3566.
LeRoy, G., Loyola, A., Lane, W. S. and Reinberg, D. (2000). Purification and characterization of a human factor that assembles and remodels chromatin. *J. Biol. Chem.* **275**, 14787-14790.
Levenson, J. M., Roth, T. L., Lubin, F. D., Miller, C. A., Huang, I. C., Desai, P., Malone, L. M. and Sweatt, J. D. (2006). Evidence that DNA (cytosine-5) methyltransferase regulates synaptic plasticity in the hippocampus. *J. Biol. Chem.* **281**, 15763-15773.
Lyu, Y. L. and Wang, J. C. (2003). Aberrant lamination in the cerebral cortex of mouse embryos lacking DNA topoisomerase IIbeta. *Proc. Natl. Acad. Sci. USA* **100**, 7123-7128.
Lyu, Y. L., Lin, C. P., Azarova, A. M., Cai, L., Wang, J. C. and Liu, L. F. (2006). Role of topoisomerase IIbeta in the expression of developmentally regulated genes. *Mol. Cell. Biol.* **26**, 7929-7941.
Martins, R. P. and Krawetz, S. A. (2007). Decondensing the protamine domain for transcription. *Proc. Natl. Acad. Sci. USA* **104**, 8340-8345.
Meek, J. and Schellart, N. A. (1978). A Golgi study of goldfish optic tectum. *J. Comp. Neurol.* **182**, 89-122.
Mondal, N. and Parvin, J. D. (2001). DNA topoisomerase IIalpha is required for RNA polymerase II transcription on chromatin templates. *Nature* **413**, 435-438.
Mondal, N., Zhang, Y., Jonsson, Z., Dhar, S. K., Kannapiran, M. and Parvin, J. D. (2003). Elongation by RNA polymerase II on chromatin templates requires topoisomerase activity. *Nucleic Acids Res.* **31**, 5016-5024.
Mumm, J. S., Williams, P. R., Godinho, L., Koerber, A., Pittman, A. J., Roeser, T., Chien, C. B., Baier, H. and Wong, R. O. (2006). In vivo imaging reveals dendritic targeting of laminated afferents by zebrafish retinal ganglion cells. *Neuron* **52**, 609-621.
Muto, A., Orger, M. B., Wehman, A. M., Smear, M. C., Kay, J. N., Page-McCaw, P. S., Gahtan, E., Xiao, T., Nevin, L. M., Gosse, N. J. et al. (2005). Forward genetic analysis of visual behavior in zebrafish. *PLoS Genet.* **1**, e66.
Nevin, L. M., Taylor, M. R. and Baier, H. (2008). Hardwiring of fine synaptic layers in the zebrafish visual pathway. *Neural Dev.* **3**, 36.
Nevin, L. M., Robles, E., Baier, H. and Scott, E. K. (2010). Focusing on optic tectum circuitry through the lens of genetics. *BMC Biol.* **8**, 126.
Polleux, F., Ince-Dunn, G. and Ghosh, A. (2007). Transcriptional regulation of vertebrate axon guidance and synapse formation. *Nat. Rev. Neurosci.* **8**, 331-340.
Robles, E., Smith, S. J. and Baier, H. (2011). Characterization of genetically targeted neuron types in the zebrafish optic tectum. *Front. Neural Circuits* **5**, 1.
Roska, B. and Werblin, F. (2001). Vertical interactions across ten parallel, stacked representations in the mammalian retina. *Nature* **410**, 583-587.
Sano, K., Miyaji-Yamaguchi, M., Tsutsui, K. M. and Tsutsui, K. (2008). Topoisomerase IIbeta activates a subset of neuronal genes that are repressed in AT-rich genomic environment. *PLoS ONE* **3**, e4103.
Scott, E. K. and Baier, H. (2009). The cellular architecture of the larval zebrafish tectum, as revealed by gal4 enhancer trap lines. *Front. Neural Circuits* **3**, 13.
Shimoda, N., Knapik, E. W., Ziniti, J., Sim, C., Yamada, E., Kaplan, S., Jackson, D., de Sauvage, F., Jacob, H. and Fishman, M. C. (1999). Zebrafish genetic map with 2000 microsatellite markers. *Genomics* **58**, 219-232.
Smear, M. C., Tao, H. W., Staub, W., Orger, M. B., Gosse, N. J., Liu, Y., Takahashi, K., Poo, M. M. and Baier, H. (2007). Vesicular glutamate transport at a central synapse limits the acuity of visual perception in zebrafish. *Neuron* **53**, 65-77.
Stuermer, C. A. (1988). Retinotopic organization of the developing retinotectal projection in the zebrafish embryo. *J. Neurosci.* **8**, 4513-4530.
Thisse, B., Pfumio, S., Furthauer, M., Loppin, B., Heyer, V., Degrave, A., Woehl, R., Lux, A., Steffan, T., Charbonnier, X. et al. (2001). Expression of the zebrafish genome during embryogenesis. ZFIN direct data submission.

Tsai, S. C., Valkov, N., Yang, W. M., Gump, J., Sullivan, D. and Seto, E. (2000). Histone deacetylase interacts directly with DNA topoisomerase II. *Nat. Genet.* **26**, 349-353.

Tsutsui, K., Sano, K., Kikuchi, A. and Tokunaga, A. (2001). Involvement of DNA topoisomerase IIbeta in neuronal differentiation. *J. Biol. Chem.* **276**, 5769-5778.

Wang, J. C. (1991). DNA topoisomerases: why so many? *J. Biol. Chem.* **266**, 6659-6662.

Warren, J. T., Jr, Chandrasekhar, A., Kanki, J. P., Rangarajan, R., Furley, A. J. and Kuwada, J. Y. (1999). Molecular cloning and developmental expression of a zebrafish axonal glycoprotein similar to TAG-1. *Mech. Dev.* **80**, 197-201.

Wearne, S. L., Rodriguez, A., Ehlenberger, D. B., Rocher, A. B., Henderson, S. C. and Hof, P. R. (2005). New techniques for imaging, digitization and analysis of three-dimensional neural morphology on multiple scales. *Neuroscience* **136**, 661-680.

Weaver, I. C., Cervoni, N., Champagne, F. A., D'Alessio, A. C., Sharma, S., Seckl, J. R., Dymov, S., Szyf, M. and Meaney, M. J. (2004). Epigenetic programming by maternal behavior. *Nat. Neurosci.* **7**, 847-854.

Woods, I. G., Kelly, P. D., Chu, F., Ngo-Hazelett, P., Yan, Y. L., Huang, H., Postlethwait, J. H. and Talbot, W. S. (2000). A comparative map of the zebrafish genome. *Genome Res.* **10**, 1903-1914.

Xiao, T. and Baier, H. (2007). Lamina-specific axonal projections in the zebrafish tectum require the type IV collagen Dragnet. *Nat. Neurosci.* **10**, 1529-1537.

Xiao, T., Roeser, T., Staub, W. and Baier, H. (2005). A GFP-based genetic screen reveals mutations that disrupt the architecture of the zebrafish retinotectal projection. *Development* **132**, 2955-2967.

Yang, X., Li, W., Prescott, E. D., Burden, S. J. and Wang, J. C. (2000). DNA topoisomerase IIbeta and neural development. *Science* **287**, 131-134.